The search for Dark Matter: SND@LHC

Bartels, Sjors

The search for dark matter: SND@LHC

THESIS

submitted in partial fulfillment of the
requirements for the degree of

BACHELOR OF SCIENCE
in
PHYSICS

Author :	S.H. Bartels
Student ID :	2647176
Supervisor :	Prof. dr. A. Boiarskyi
Daily supervisor:	Dr. M. Ovchynnikov
2^{nd} corrector :	Dr. S.P. Patil

Leiden, The Netherlands, July 13, 2022

The search for dark matter: SND@LHC

S.H. Bartels

Huygens-Kamerlingh Onnes Laboratory, Leiden University
P.O. Box 9500, 2300 RA Leiden, The Netherlands

July 13, 2022

Abstract

This paper considers how the SND neutrino detector at the Large Hadron Collider, CERN, may probe light dark matter. To this end, the leptophobic portal is considered (mostly with a dark matter mass of 20 MeV). After a review of the sensitivity of the current SND configurations, two alternative configurations are considered: one in the same pseudorapidity range as the current experiment, the other further off-axis. While the former will have a higher sensitivity than the current experiment, for the latter this depends on the mediator mass. For a mediator mass of 7 GeV, the sensitivity of the off-axis configuration is higher than the sensitivity of the current experiment and the other alternative configuration.

Contents

1 Introduction **1**

2 Beyond the Standard Model: Dark Matter **3**
2.1 Standard Model 3
2.2 Beyond the Standard Model 4
2.3 Dark Matter 5
2.4 Lee-Weinberg bound 6
2.5 Light Dark Matter 6

3 SND@LHC **9**
3.1 Detector 9
3.1.1 Veto plane 9
3.1.2 Target region 10
3.1.3 Muon system 11
3.1.4 Event reconstruction 11
3.2 Dark Matter detection 12
3.2.1 Elastic signature 12
3.2.2 NC/CC ratio 14

4 Leptophobic Dark Matter **17**
4.1 Leptophobic portal 17
4.2 Production channels 18
4.2.1 Interaction radius 19
4.2.2 Proton content 19
4.2.3 Proton bremsstrahlung 19
4.2.4 Drell-Yan process 20
4.2.5 Meson decay 20
4.2.6 Total production 21

Version of July 13, 2022– Created July 13, 2022 - 16:12

4.3 Constraints 22
4.3.1 Direct detection: CRESST-III 23
4.3.2 MiniBooNE 23
4.3.3 CDF 23
4.4 Reach of SND 23

5 Advanced Configurations of SND 27
5.1 Events 27
5.2 Advanced configurations 28
5.2.1 $\text{AdvSND}_{\text{far}}$ 28
5.2.2 Cross section 29
5.2.3 Geometric Acceptance 31
5.2.4 Average cross section 32
5.2.5 $\text{AdvSND}_{\text{near}}$ 32
5.2.6 Sensitivity 33
5.3 Discussion 34

6 Conclusion 37

A Pseudorapidity 41

B m_χ limit CRESST-III 43

Chapter 1

Introduction

During the twentieth century, the standard model of elementary particle physics (Standard Model, SM) has been developed. At its core, it is a mathematical framework to explain observations/experiments. With the discovery of the Higgs boson in 2012, all predictions based on the standard model had been measured/confirmed. Although experiments at particle colliders can be explained by the standard model, there remain questions. There are phenomena that cannot be explained by the standard model. Therefore, the standard model is incomplete. This research focuses on dark matter, the term for one of the phenomena not explained by the standard model. In 1932 already, Oort concluded that there must be mass in galaxies that we cannot see: it does not emit light. Light, photons, being the result (mediator) of the electromagnetic force, this 'dark matter' does not directly interact electromagnetically.* Therefore, for decades already, the question is what constitutes this dark matter and how we can measure/detect it. Despite many searches, these questions have not been answered yet. Some look for particles with very high mass; so high that we cannot see them yet because our current particle accelerators do not provide enough center-of-mass energy. Recent theories, however, propose to look for lighter particles, instead, relying on them interacting so feebly (even weaker than typical weak force interactions) with standard model particles that we have not seen them yet. Therefore, the particles predicted by these theories are referred to as feebly interacting particles, FIPs [2].
Another problem of the Standard Model is that it predicts neutrinos to be massless. Contrary to this prediction, experiments have shown that in reality, neutrinos do have a (very tiny) mass. At CERN, Geneva, a new de-

*Although an observed 3.5 keV line has been suggested to originate from dark matter [1].

Version of July 13, 2022– Created July 13, 2022 - 16:12

tector, the Scattering and Neutrino Detector at the Large Hadron Collider (SND, SND@LHC) is used to investigate neutrino scatterings during Run 3 of the LHC. However, it may also be used to probe dark matter candidates.
In this paper, following [3], I will detail how the SND detector may probe leptophobic light dark matter. To this end, the workings of the detector will be explained first. Then the leptophobic portal is considered, to see how much of the parameter space SND covers. Lastly, I will discuss two alternative configurations of the detector, $AdvSND_{far}$ and $AdvSND_{near}$ that have been proposed for Run 4 of the LHC. Before all else, I will first provide the reader with some background information on the standard model and dark matter.

Version of July 13, 2022– Created July 13, 2022 - 16:12

Chapter 2

Beyond the Standard Model: Dark Matter

2.1 Standard Model

At its core, the Standard Model of Particle Physics is a mathematical framework to explain observations/experiments in particle physics. Mathematically, it is a local symmetry group describing the electromagnetic and weak nuclear forces (together the electroweak force) as well as the strong nuclear force. This gauge group is the direct product U(1)xSU(2)xSU(3) of the circle group U(1) and the special unitary groups SU(2) and SU(3). SU(3) is the symmetry group associated with the strong force (described by quantum chromodynamics). It has dimensionality 8, which corresponds to there being 8 independent colour states for gluons, the force carries of the strong force. Those interact with the 6 quarks of the model as seen in Fig. 2.1 and their antiparticles.
The U(1) and SU(2) groups are connected to the electromagnetic and weak nuclear forces, but not as straightforwardly. The U(1) group is connected to one boson, B. The SU(2) group has dimensionality 3 and gives rise to the three bosons $W_{1,2,3}$. However, we know that the mediator of the electromagnetic interaction is the photon γ and the mediators of the weak interaction are the $Z^0, W^{\pm}$ bosons. These emerge because of spontaneous symmetry breaking from U(1)xSU(2). The B and W_3 bosons mix to produce γ and Z^0, both having no electric charge. Mixing of the $W_{1,2}$ bosons yields the electrically charged $W^{\pm}$ bosons. This symmetry breaking is theoretically associated with the Higgs mechanism, which gives mass to the $Z^0, W^{\pm}$ particles. It requires an additional quantum field to be introduced

into the theory and an additional boson: the Higgs boson. In 2012, a particle that is believed to be the Higgs boson was discovered at CERN, at the time the last particle of the Standard Model to be discovered.
The photon interacts with quarks (which have not only colour charge but also electric charge) as well as the charged leptons: the electron, muon and tauon and their antiparticles. The other leptons, the neutrinos, are electrically neutral and only interact with the W and Z bosons. All other fermions (so quarks and leptons) interact with the weak interaction too. The elementary particles of the Standard Model are depicted in Fig. 2.1.

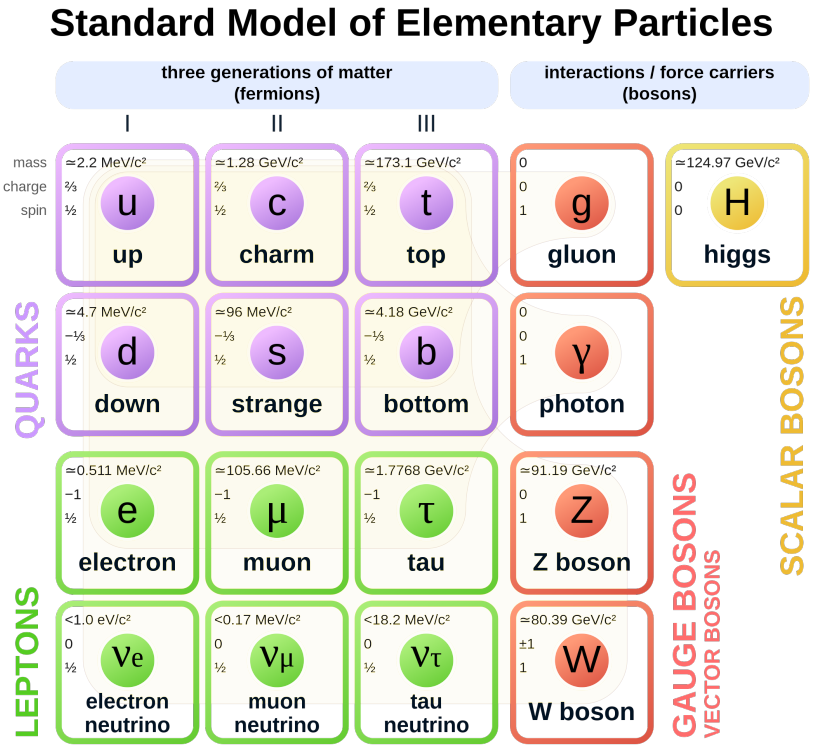

Figure 2.1: *Standard Model of particle physics. The figure shows the particles as well as which fermions interact with which mediators. Figure taken from Wikipedia.*

2.2 Beyond the Standard Model

The Standard Model is very successful in the sense that it agrees with the outcome of collider experiments so far. However, certain phenomena are

observed that cannot be explained by the (current) Standard Model. Such phenomena are called Beyond the Standard Model (BSM) problems, as they require a modification/addition to the current model: the Standard Model is not complete. These phenomena include the baryon asymmetry in the Universe, neutrino oscillations and dark matter (as discussed in [4]).
The baryon asymmetry problem comes down to there being more baryonic matter than antimatter in the Universe. However, one intuitively assumes that the Big Bang should have produced just as much matter as antimatter. Either this was not so, or asymmetry has occurred later in the Universe's evolution. In any case, it cannot be explained by the Standard Model.
The Standard Model predicts neutrinos to be massless particles that have a certain lepton flavor (electron, muon, tau). The detection of neutrinos must be through weak force interactions as the neutrinos only interact with the Z and W bosons, such that what is detected is actually the lepton flavour. However, experiments have shown that in reality, neutrinos are not massless and they can transition between lepton flavours. The latter phenomenon is known as neutrino oscillations. The idea is that the lepton flavour states are linear combinations of the mass states. This cannot be explained by the Standard Model.

2.3 Dark Matter

The BSM problem that will be relevant for the rest of this paper is the dark matter problem. In 1932 Oort looked at stellar motion in the Milkyway. Equating the gravitational force and the centripetal force, one can predict the velocity of stars moving around the galactic centre as a function of the the mass in the galaxy and the distance from the centre. Oort's observations, however, showed that the velocity of the stars was higher than could be expected from the visible matter in the galaxy. Therefore, he concluded there must also be matter that we cannot see: dark matter. Zwicky came to the same conclusion on the scale of a galaxy cluster in 1933. Since then, evidence has been piling up that there must be invisible mass. In the Standard Model, only neutrinos are electrically neutral matter particles. However, their mass is not high enough to account for the total amount of invisible matter. Therefore, the Standard Model cannot explain the dark matter existence.

2.4 Lee-Weinberg bound

Many proposed solutions to explain the dark matter problem involve weakly interacting massive particles (WIMPs): as they are massive, they may account for the invisible mass in galaxies, but because they do not interact via the electromagnetic force, they are dark matter (DM) particles and because they do not interact via the strong force they are called weakly interacting. Such particles were first proposed by Lee and Weinberg [5].
In their paper, they derive a lower bound for the mass of such particles, therefore called the Lee-Weinberg bound. The idea is that the DM particles were in thermal equilibrium through the annihilation $\chi + \overline{\chi} \leftrightarrow SM + SM$ in the early Universe. This process has an interaction rate Γ_{int}. As the Universe expanded, the density of DM particles decreased, such that Γ_{int} decreased. At some point, the annihilation rate was lower than the rate of expansion of the Universe $H = \frac{\dot{a}}{a}$, $\Gamma_{int} < H$ such that the annihilation did not take place (as much as before) anymore. Therefore, the amount of WIMPs in the present is determined by the density of the Universe when $\Gamma_{int} = H$. This leads to the equation [4]

$$\Omega_\chi h^2 < \sigma v >= 3 \cdot 10^{-27} cm^3/sec \tag{2.1}$$

where the interesting term is the thermal average of the cross section times the relative velocity $< \sigma v >$ as it scales as $< \sigma v > \sim G_F^2 m_\chi^2$ so

$$\Omega_\chi \sim G_F^{-2} m_\chi^{-2} \tag{2.2}$$

The Fermi constant G_F scales with the mass of the W boson as $G_F \sim M_W^{-2}$. Therefore, eq. 2.1 links the number density of dark matter particles (Ω_χ) to the mass of the DM particle (m_χ) and the mass of the W boson, which is known.

As the number density of DM particles cannot exceed the total number density of the Universe, determining the latter constraints the mass of the DM particle. The Lee-Weinberg bound is $m_\chi > 5\ GeV$ [4]. So by this reasoning, there can be no WIMP particle with a mass lower than about 5 GeV.

2.5 Light Dark Matter

Nevertheless, there is a way around this constraint, as it only applies to particles weakly interacting with SM particles. The idea is that there may

be a currently unknown mediator between the DM particles and SM particles. If this is the case, the scaling with the mass of the W boson in the Fermi constant is to be replaced by the mass of this new mediator, so [4]

$$\Omega_\chi \sim \frac{m_{mediator}^4}{m_\chi^2} \tag{2.3}$$

Of course the upper boundary on Ω_χ still holds, but if $m_{mediator} < m_W$, then m_χ is not as constrained anymore. Such a model therefore allows for DM particles with a mass below the Lee-Weinberg bound of 5 GeV. DM particles with $m_\chi < 5\ GeV$ are called Light Dark Matter (LDM).

Version of July 13, 2022– Created July 13, 2022 - 16:12

Chapter 3

SND@LHC

During Run 3 of the Large Hadron Collider (LHC) at CERN, a new detector is used: the Scattering and Neutrino Detector (SND, SND@LHC). The detector is positioned in the TI18 tunnel, 480 m from the ATLAS interaction point. Because the detector is positioned just slightly off-axis, with pseudorapidity range $7.2 < \eta < 8.6$, it will study the scattering of neutrinos with high energy [3].*
However, the detector may also be able to detect particles scattering similarly to neutrinos; light dark matter particles interacting with SM particles for instance.

3.1 Detector

Although the details are beyond the scope of this paper, a brief explanation of the detector is now included. This part of the paper is based on the information of the SND collaboration provided in their letter of intent [6] and technical proposal [7]. Fig. 3.1 shows the layout of the detector. From upstream to downstream, it consists of the veto plane, target region and muon system. Its total length is 2.6 m, the area of the target region 39 x 39 cm^2.

3.1.1 Veto plane

As the goal of the experiment is to detect/measure neutrinos, and neutrinos are electrically neutral, the first part of the SND detector is a veto

*Please see Appendix A for an explanation of the pseudorapidity η.

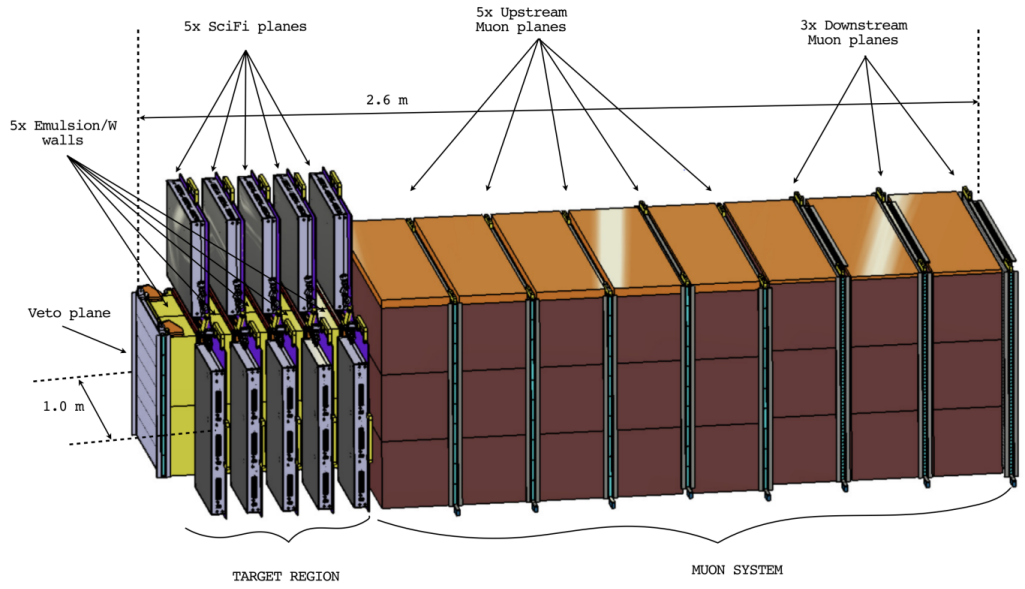

Figure 3.1: *Layout of the SND detector. The detector consists of the veto plane, the target region (consisting of 5 emulsion cloud chambers and scintillating fibre plates) and the muon system (consisting of 8 iron blocks and scintillator planes). Figure taken from [7].*

system. The veto system consists of two planes of scintillator bars and silicon photomultipliers, tagging charged particles reaching the detector (especially muons).

3.1.2 Target region

Following the veto system is the target region. It consists of five bricks of emulsion cloud chambers(ECC) followed by scintillating fibre plates. The emulsion bricks consist of 60 emulsion films interleaved with 59 tungsten plates. The actual target, tungsten, is a very dense material and the total target mass is about 800 kg. The emulsion films are vertex detectors with micrometric resolution and together show the tracks of charged particles. As the measurements on these bricks have to be performed by studying them with an optical microscope, they are planned to be replaced every six months. Tau leptons will be identified by studying the vertices in the emulsion.
The scintillating fibre plates (SciFi) record time and position stamps for charged particles that pass. They provide missing information about the electromagnetic and hadronic showers that are visible in the ECC: their

energy. The measurements of the SciFi plates can be used to disentangle all the tracks/events recorded by the emulsion films and link events from successive bricks. Together, the emulsion bricks and the SciFi plates form an electromagnetic calorimeter. An electron produced by neutrino scattering creates an electromagnetic shower which is detected by the electromagnetic calorimeter.

3.1.3 Muon system

The most downstream component of the SND detector is the muon system. It consists of 8 iron blocks and scintillator planes. The iron slows the particles down. Additionally, iron can be magnetised, such that charged particles will be deflected. By measuring the deflection with the scintillator planes, their energy can be determined. This part of the detector is called the muon system because especially muons will be able to reach it: because they are so massive and interact way less with other particles than for instance an electron, most of the muons created in the target section will penetrate the muon system.
Because of all the iron (8 blocks each 20 cm thick), the muons will be slowed down and their tracks measured by the plates. Because almost all other particles will be stopped by the iron, if a particle reaches the last three scintillating planes it can be selected as a muon. Together with the scintillating fibre plates in the target region, the muon system scintillator planes form a hadronic calorimeter.

3.1.4 Event reconstruction

As the electronic detectors (veto plane, SciFi plates in target region and scintillator planes in muon system) transmit their signals continuously during the run of the experiment, this data may be analysed during the run of the experiment. Using these measurements, one can already reconstruct electromagnetic showers, identify muon candidates and get an estimate of the neutrino energies. Analysis of the emulsion target provides crucial information for identifying tau lepton events. The tracks also provide additional information on the energies of the incoming particles (the higher the energy, the narrower a shower). Furthermore, one can distinguish electromagnetic showers by photons from those by electrons, as the emulsion films show a displaced vertex for the photon conversion process due to their micrometric accuracy.

3.2 Dark Matter detection

Although the SND detector primarily aims to detect neutrinos, it may probe dark matter particles as well. In this paragraph, two signatures for dark matter particles scattering off protons in the target are discussed.

3.2.1 Elastic signature

Neutrinos scattering off of particles in the target material can happen either elastically (the final state of the nucleon does not change) or inelastically (the nucleon breaks up, creating a hadronic shower). Which of the two is dominant depends on the mediator mass. Elastic scattering is subdominant for mediator masses $m_{mediator} \gtrsim 1GeV$. Because neutrino scattering is determined by the weak force, this is the case for neutrino scattering, as the mass of the Z boson is about 91 GeV and the mass of the W boson is about 80 GeV. Therefore, very few elastic neutrino scattering events are expected at SND@LHC. In fact, only 1.7 events are expected during the whole run of SND@LHC [3].

Elastic vs inelastic cross sections

The reason is that the elastic differential cross section has an additional term as compared to the inelastic differential cross section (discussion based on [3]). Because for elastic interactions the proton is considered as a whole particle, the proton form factor D_p shows up in the vertex, thus entering the cross section squared. In terms of the momentum transfer Q and mediator mass (m_V in the equation);

$$\begin{aligned} \frac{d\sigma_{el}}{dQ^2} &\sim \frac{1}{(Q^2+m_V^2)^2} D_p^2(Q^2) \\ \frac{d\sigma_{inel}}{dQ^2} &\sim \frac{1}{(Q^2+m_V^2)^2} \end{aligned} \tag{3.1}$$

The proton form factor scales as

$$D_p(Q) \sim \frac{1}{(1+\frac{Q^2}{0.71GeV^2})^2} \tag{3.2}$$

From eqs. 3.1 and 3.2 it can be seen that the elastic cross section goes to zero for momentum transfers higher than 0.843 GeV. The reason is that

this is the momentum transfer associated with an interaction radius the size of the proton. For higher momentum transfer, the interaction radius is smaller than the radius of the proton, such that the interaction takes place on a smaller scale than the proton as a whole. This means that instead of elastic scattering, inelastic scattering is being considered.
Therefore, the integration interval to compute the total cross section is effectively limited to 0.843 GeV in the elastic case. In both the elastic and inelastic cases, the interval is limited by the mediator mass. Combining these two statements, the integration interval for (deep) inelastic scattering extends to the mediator mass, while the integration interval for elastic scattering extends to min[mediator mass, 0.843 GeV]. Therefore, elastic scattering is suppressed for mediator masses higher than about 1 GeV, while lighter mediator masses lift this suppression. Fig. 3.2 shows a plot that gives a good idea of the ratio between the elastic and inelastic scattering cross sections for different mediator masses.

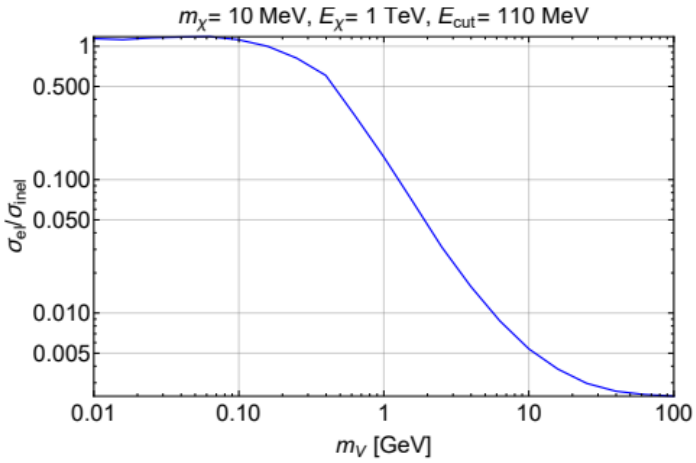

Figure 3.2: *Ratio between cross sections of elastic and inelastic scattering $\sigma_{el}/\sigma inel$ for a model with mediator mass m_V. The plot is based on a DM mass $m_\chi = 10\ MeV$ and energy $E_\chi = 1\ TeV$. Additionally, the proton is assumed to have the minimal kinetic energy of 110 MeV, such that it could be detected. Figure taken from [3].*

Now suppose that the mediator mass of the leptophobic dark matter model that is considered in this paper is below the GeV level. Dark matter particles scattering off protons would then be an explanation for detecting elastic scattering events. As such, an excess of elastic scattering events (seen as hadronic showers) would be a hint for the existence of light dark matter particles.

Experimental problems

As elastic scattering of neutrinos/dark matter off of protons leaves the protons intact, identifying these events could happen by detecting the scattered protons. However, the scattered protons will have energies below the 1 GeV limit. Because they have such low energies, they are absorbed in the target region before reaching the SciFi detectors. Therefore, the elastic signature will only be visible in the emulsion films (which require the protons to have kinetic energies above 110 MeV) [3]. Unfortunately, the background may pose a problem. Other cascades may mimic proton tracks. Because it is unknown how many tracks from other particles may mimic the desired proton tracks, it is unclear whether the elastic signature would yield accurate results.

3.2.2 NC/CC ratio

Fortunately, elastic scattering is not the only possible signature of dark matter. Apart from the elastic/inelastic distinction, one can also distinguish between neutral-current (NC) and charged-current (CC) interactions. Charged-current interactions are characterised by an exchange of a $W^{\pm}$ between the neutrino and the nucleon, while neutral-current events involve the exchange of a Z boson. For the following discussion, a mediator mass (for the coupling between DM and SM particles) higher than 1 GeV is assumed, such that (deep) inelastic scattering (DIS) is dominant for DM scattering as well.
A DM particle scattering of a proton in the target mimics NC neutrino events. Therefore, one would like to know how many of those events take place in the detector. However, the amount of neutrino events in the detector is quite uncertain, such that just looking at the amount of detected NC events and seeing if this is higher than the expected amount of NC neutrino events is not very useful.

Although the amount of NC neutrino events during the run of SND@LHC is quite uncertain, the ratio between NC and CC neutrino events is determined by the standard model. One of the goals of SND is to measure this ratio, as a consistency check for the standard model. However, if there are enough DM scattering events, there will be relatively more NC events registered (as DIS DM events mimic NC neutrino-nucleon interactions). Therefore, an NC/CC ratio that is higher than predicted by the SM may indicate DM particles.

Assuming as many neutrinos as anti-neutrinos reach the detector, the NC/CC ratio is given by [8]

$$P = \frac{\sigma^{\nu}_{NC} + \sigma^{\bar{\nu}}_{NC}}{\sigma^{\nu}_{CC} + \sigma^{\bar{\nu}}_{CC}} \tag{3.3}$$

This can be shown to be [9] (for a derivation, see [10]):

$$P = \frac{1}{2}\{1 - 2sin^2\theta_W + \frac{20}{9}sin^4\theta_W - \lambda(1 - 2sin^2\theta_W)sin^2\theta_W\} \tag{3.4}$$

where θ_W is the Weinberg angle (also called the weak-mixing angle as it describes the mixing between the electromagnetic and weak interaction in the standard model) and λ is a measure to correct the equation for an unequal amount of protons and neutrons in the target. For tungsten, $\lambda \approx 0.040$, so (using $\theta_W \approx 28^\circ$) $P \approx 0.33$ [3].

There are a few errors on this P. First of all, there is the statistical error (determined by the amount of neutrino interactions), which will be less than 5 %. A systematic error, up to 10%, is caused by CC events being recognised as NC events because the resulting lepton is not identified as such. Lastly, there is an error of less than 5% due to the asymmetry between neutrino and anti-neutrino spectra. The total (experimental) uncertainty in P is about 10 % [7].

If we assume the 450 NC neutrino events that has been simulated for SND in [7], the amount of LDM inelastic scattering events needed for the desired 2σ confidence level can be computed. Because the amount of NC events is Poisson distributed, one also has to consider a contribution $\sigma_{Poisson} = \sqrt{450}$. The experimental uncertainties amount to an error $\sigma_{experimental} = 0.1 \cdot 450 = 45.0$. Adding the uncertainties quadratically, the total is given by:

$$\begin{aligned} \sigma^2_{total} &= \sigma^2_{Poisson} + \sigma^2_{experimental} \\ \sigma_{total} &= \sqrt{450 + 45.0^2} \end{aligned} \tag{3.5}$$

Therefore, a 2σ confidence level that the ratio measurements indicate a deviation from the theoretical NC/CC ratio (thus hinting at the existence of DM[†]) requires ≈ 100 LDM inelastic scattering events [3].

[†]A deviation of this ratio in itself is not evidence of dark matter, it could also be that the SM needs adjusting on another level. However, evidence for DM may be further found by studying the kinematics and topology of the final state hadrons, which are different for neutrino events and DM events.

Version of July 13, 2022– Created July 13, 2022 - 16:12

Chapter 4

Leptophobic Dark Matter

4.1 Leptophobic portal

The dark matter particle considered in this paper is a scalar particle, χ, that couples to SM particles via a leptophobic portal. A leptophobic portal means that the DM particle has an interaction with a vector mediator, V, that does not interact with leptons (directly), but it does interact with the baryon current $J^B_\mu = \frac{1}{3}\overline{q}\gamma_\mu q$. In other words, the interactions is with quarks (pairs, $\overline{u}u$, $\overline{d}d$, etc.). The reason why a leptophobic portal is considered is that other experiments are more efficient at probing the parameter space if the DM particle couples to leptons. For a leptophobic portal, however, SND@LHC may probe an unexplored part of the parameter space. The Lagrangian is given by :

$$\mathcal{L}_{leptophobic} = -g_B V^\mu J^B_\mu + g_\chi V^\mu (\partial_\mu \chi^\dagger \chi + \chi^\dagger \partial_\mu \chi) \tag{4.1}$$

The relevant parameters in this model are:

- m_V the mass of the mediator
- m_χ the mass of the DM particle
- $\alpha_B = \frac{g_B^2}{4\pi}$ the coupling of the mediator to the baryon current
- $\alpha_\chi = \frac{g_\chi^2}{4\pi}$ the coupling of the mediator to the DM particles

When performing calculations or plotting figures, it is common to fix α_χ and m_χ, keeping α_B and m_V as parameters. Often, $\alpha_\chi = \alpha_B$ or $\alpha_\chi = 0.5$ is taken. For m_χ, $m_\chi = m_V/3$ is regularly used. In this paper, as we are

interested in LDM particularly, $m_\chi = 20\ MeV$ is considered unless stated otherwise.

4.2 Production channels

The DM particles may be produced by pair production from the mediator: $V \to \chi\overline{\chi}$. Therefore, we have to consider how the mediator can be produced. Because the LHC is used as a proton accelerator, production channels from protons will be considered. The three channels considered are (as described in [11]):

- Proton bremsstrahlung: $p + p \to V + X$
- Drell-Yan process: $q + \bar{q} \to V + X$
- Decay of light, unflavoured mesons: $\pi^0, \eta \to V\ +\ \gamma$

Their diagrams are given in Fig. 4.1.

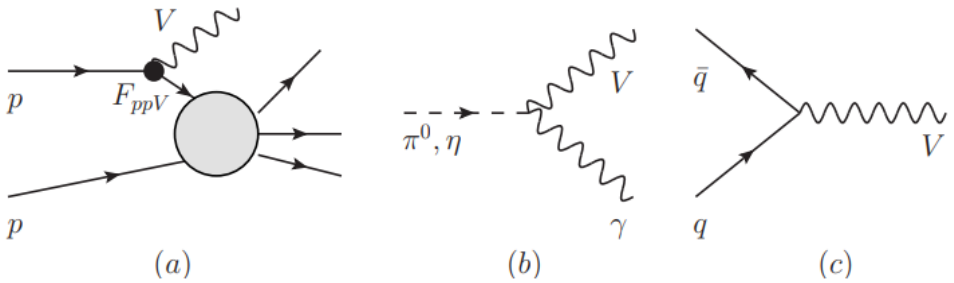

Figure 4.1: *The diagrams of the three channels considered for producing the mediator of the leptophobic portal. (a) proton-proton bremsstrahlung, (b) π^0, η decay, (c) Drell-Yan process. Figure taken from [3].*

The first two (a and c in Fig. 4.1) are direct production channels: the mediator is produced by two interacting protons or quarks from protons. The difference is that bremsstrahlung is an elastic interaction, while the Drell-Yan process is inelastic. Which of the two takes place (dominantly) is determined by the mediator mass m_V. The third is an indirect channel, which requires the production of the mesons first.

In order to understand the two direct production channels, some remarks have to be made on the interaction radius and proton content.

4.2.1 Interaction radius

First of all, the scale at which the interaction takes place, called the interaction radius r_{int} here, is determined by the momentum transfer of the interaction. The interaction radius scales with the momentum transfer as $r_{int} \sim \frac{1}{Q}$. To produce the mediator, a momentum transfer of the mediator mass is minimally required. Thus, the momentum transfer Q needed to produce the mediator is $Q = m_V$. Therefore, a larger m_V means a smaller r_{int}. Expressed in energy scales, the proton radius is $r_{proton} \sim 1GeV^{-1}$. If $r_{int} < r_{proton}$, the interaction takes place on a smaller scale than the proton as a whole: one is actually considering an inelastic process.

4.2.2 Proton content

Although for the standard model a proton is considered to consist of 3 quarks (2 up, 1 down), it is actually a collection of many particles: there is a sea of quarks and gluons, together called partons. The three quarks that we describe the proton with are just the valence quarks that describe the (flavour) symmetry properties that are considered in the standard model. The quarks are bound together by the strong force.
For low momentum, the strong coupling constant is high, such that the quarks are strongly bound and the resulting particle can/must be treated as a hadron. This is known as confinement. However, the strong coupling constant decreases for higher momentum. This is known as asymptotic freedom: for very high momentum, the quarks are not bound as strongly, which allows for them to be treated separately by perturbation theory. The boundary where perturbation theory breaks down (i.e. the strong coupling is strong enough to consider the proton as a whole) is around a momentum (of the proton) of 1 GeV.

4.2.3 Proton bremsstrahlung

Let us now consider proton-proton bremsstrahlung. The question immediately rises how this process can even create the mediator V, as the Lagrangian eq. 4.1 includes quarks, while we are treating the proton as a whole here. The solution is to introduce an effective interaction, such that the vertex can be considered as:

$$< p(\vec{k})|\overline{q}\gamma^{\mu}q|p(\vec{k}^{'}) > V_{\mu} = \overline{p}\gamma^{\mu}p \cdot F_{ppV}((k-k^{'})^2)V_{\mu} \tag{4.2}$$

where the from factor F_{ppV} is introduced. Because $k^{\mu} = k^{'\mu} + k_V^{\mu}$ we have $Q^2 = (k-k^{'})^2 = k_V^2 = m_V^2$. In this notation we can say [3]:

$$\begin{aligned} F_{ppV}(Q^2 \to 0) &\approx g_{ppV} \\ F_{ppV}(Q^2 >> \frac{1}{r_p^2}) &\to 0 \end{aligned} \tag{4.3}$$

where g_{ppV} is just some constant.
From this expression, it is once again clear that the bremsstrahlung channel only contributes significantly if the mediator mass is smaller than the inverse of the proton radius, so $m_V \lesssim 1GeV$. If it is bigger, the momentum transfer required to produce the mediator forces us to consider the inelastic process instead.

4.2.4 Drell-Yan process

The dominant deep-inelastic production process is the Drell-Yan process. This process could create the mediator if its mass is higher than 1 GeV. However, we must take into account that although the typical energies of the protons produced at the LHC, we are now considering interactions with partons (quarks) instead of the proton as a whole: the energy of the interacting quarks has to be high enough to produce the mediator. This means that the parton distribution function (PDF, $f(x, Q)$) must be considered: the probability to find a parton with a certain fraction of the protons energy (x) for a certain scale of the process Q, the invariant mass of the process. Generally, the PDF takes the following form: it starts relatively high at low x, but quickly decreases at some point. Therefore, although at LHC, the proton energy is about $E_p = 6.5\ TeV$, there will be few quarks with such high energies. As a result, the amount of produced mediators by the Drell-Yan process will decrease for increasing mediator mass m_v.

4.2.5 Meson decay

Because V couples to the baryon current ($\overline{u}\gamma^\mu u + \overline{d}\gamma^\mu d$ (+...)) by definition (see eq. 4.1), it couples (directly) to flavourless mesons. The two most important mesons to be considered are the electrically uncharged pion and the (regular) eta meson, as both are flavourless

$$\pi^0 = \frac{u\overline{u} - d\overline{d}}{\sqrt{2}}, \eta = \frac{u\overline{u} + d\overline{d} - 2s\overline{s}}{\sqrt{6}}$$

and relatively light

Version of July 13, 2022– Created July 13, 2022 - 16:12

$$m_{\pi^0} \approx 135\ MeV, m_\eta \approx 548\ MeV$$

One may wonder why other flavourless mesons such as

$$\eta^{'} = \frac{u\bar{u} + d\bar{d} + s\bar{s}}{\sqrt{3}}, \eta_c = c\bar{c}, \eta_b = b\bar{b}$$

are not so important. The reason is their masses

$$m_{\eta'} \approx\ 958MeV, m_{\eta_c} \approx 2.98\ GeV, m_{\eta_b} \approx 9.39\ GeV$$

As was said before, the meson decay channel is indirect as the mesons have to be produced from protons first. This explains why only the lighter mesons are relevant. The mass of the $\eta^{'}$ particle already approaches 1 GeV and we have previously seen that for such energies, we have to consider quarks instead of the proton as a whole. The heavier mesons, therefore, are produced via an analogue of the Drell-Yan process. This means that (because of the parton distribution function) the heavier the meson, the less will be produced and only the production of the lighter mesons is significant. Apart from this, the production process for the heavier mesons is sub-dominant to the Drell-Yan process, such that for higher mediator masses, Drell-Yan would be more relevant anyway.

In the meson decay $\pi^0, \eta \to V + \gamma$, only mediators with $m_V < m_{\pi^0}, m_\eta$ can be produced (a higher mass would violate conservation laws).

4.2.6 Total production

Considering the production channels above, one can determine how many DM particles will be produced at the LHC in the direction of the SND detector. This has been done by [3]. Their results are given in Fig. 4.2.

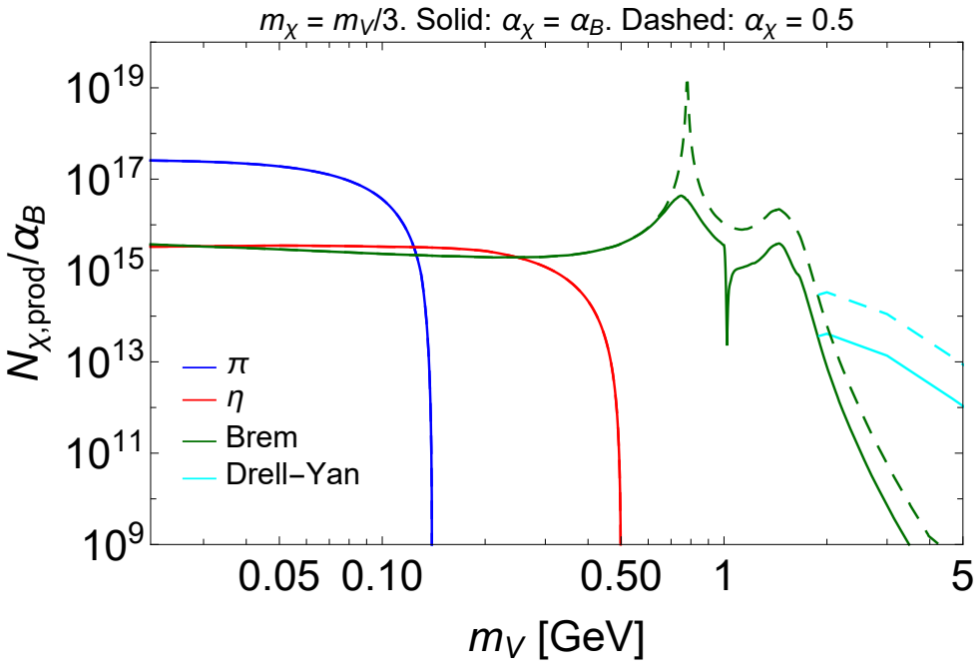

Figure 4.2: *The total amount of produced χ particles in the direction of the SND detector by the considered production channels, plotted against the mediator mass m_V for an integrated luminosity $\mathcal{L} = 150 fb^{-1}$, assuming $m_\chi = m_V/3$. Up to $m_V = m_{\pi^0} \approx 135\ MeV$, π_0 decay is the dominant production mechanism. Although production from η decay may happen up to $m_V = m_\eta \approx 548\ MeV$, proton bremsstrahlung is dominant from about $m_V \approx 0.3\ GeV$. Drell-Yan production takes over around $m_V \approx 2\ GeV$. The dashed line represents $\alpha_\chi = 0.5$, the solid line $\alpha_\chi = \alpha_B$. The three wiggles around $m_V \approx 782\ MeV, 1020\ MeV, 1.7\ GeV$ originate from mixing of the mediator with mesons ω and ϕ. This has not been discussed in this paper, but for more information see [3]. Figure taken from [3].*

4.3 Constraints

SND@LHC is not the first experiment to probe the leptophobic portal. Some constraints from previous experiments are worth discussing, based on [3]. After this short summary, Fig. 4.3 shows the constraints for 2 parameter choices.

4.3.1 Direct detection: CRESST-III

The CRESST-III experiment is currently the most sensitive direct detection experiment (for DM mass up to 1.8 GeV) that looks for scattering of DM particles off nuclei. It is very sensitive because the energy threshold for the recoil energy is only 30.1 eV. This is important, as the energy threshold determines the lowest possible DM mass m_χ for which events would be registered. The DM particles that could be measured originate from the DM halo of the Milkyway, which has an escape velocity of $v_{esc}^{Milkyway} \approx 544\ km/s$. Together with the energy threshold of 30.1 eV this leads to the constraints from the results of CREST-III being valid for $m_\chi \gtrsim 160\ MeV$ [12]. For a detailed derivation (and discussion) of this 160 MeV limit, please see Appendix B.

4.3.2 MiniBooNE

Quite similar to the SND@LHC experiment, MiniBooNE is supposed to detect scatterings of DM particles off nucleons [13]. However, at MiniBoo, a proton beam collides with a fixed target, with COM energy ($\sim$ 4 GeV) way lower than at LHC ($\sim$ 13 TeV). Therefore, MiniBooNE is efficient only for studying light mediators ($m_V \sim 1$ GeV). As a result, the constraints from MiniBooNE instantly drop around 1.5 GeV. On the other hand, there are way more protons at MiniBooNE, such that it probes low mass mediators more efficiently than SND. The constraints that the MiniBooNE results impose on the parameter space are reflected in Figure 4.3.

4.3.3 CDF

The Collider Detector at the Fermilab (CDF) has probed the monojet signature of DM particles ($p\overline{p} \rightarrow jet + \chi\overline{\chi}$) [14]. The DM particles would be indicated by missing transverse momentum p_T. Unfortunately, a large missing transverse momentum ($p_T \sim 100$ Gev) is required for this type of experiment. Since we are considering light mediators ($\mathcal{O}(1\ GeV)$), the monojet signature does not add much to the other constraints. Nevertheless, as can be seen in Fig. 4.3, it is taken into account.

4.4 Reach of SND

One can now consider the reach of the SND experiment to see whether it adds to the currently known constraints (and thus is an interesting ex-

periment from a DM point of view). To do so, one has to consider how the amount of DM particles produced in the direction of the detector (see Fig. 4.2) translates to the amount of events to can be detected and so the sensitivity of the experiment. In order to have maximum impact (smallest excluded domain), one would like to consider a high α_χ. Following literature, $\alpha_\chi = 0.5$ is considered.

Number of events

The total number of events taking place in the detector can be calculated as $N_{events} = N_{prod} \cdot \epsilon_{geom} \cdot P_{scat}$ with:

- N_{prod} the total amount of χ particles produced at LHC, $\sim \alpha_B$
- ϵ_{geom} the geometrical acceptance of the target (SND), which is a function of kinematics and the specific production channel that is considered, $\sim f(m_\chi, m_V)$
- P_{scat} is the probability the DM particle scatters off a proton, $\sim \alpha_B \alpha_\chi f(m_\chi, m_V)$

The last scaling with $\alpha_B \alpha_\chi$ is because $P_{Scat} \sim \sigma \sim |\mathcal{M}|^2 \sim (g_\chi g_B)^2 \sim \alpha_B \alpha_\chi$ as $\alpha_{B,\chi} = \frac{g_{B,\chi}^2}{4\pi}$.

The requirement that determines the sensitivity of SND for inelastic scattering is the $N_{events}^{LDM,inel} \approx 100$ that was calculated in 3.2.2. For elastic scattering (for which 1.7 elastic neutrino scattering events were expected, 3.2.1), the plot is made for $N_{events}^{LDM,el} = 10$.

In their paper, Boyarsky et al. plot the constraints and sensitivity of SND@LHC in 4 figures. They choose $\alpha_\chi = \alpha_B$ (for which $N_{events} \sim \alpha_B^3$) and $\alpha_\chi = 0.5$ (for which $N_{events} \sim \alpha_B^2$), as well as $m_\chi = m_V/3$ and $m_\chi = 20\ MeV$ as fixed parameters for these plots [3]. The two plots for $\alpha_\chi = 0.5$ are shown in Fig. 4.3.

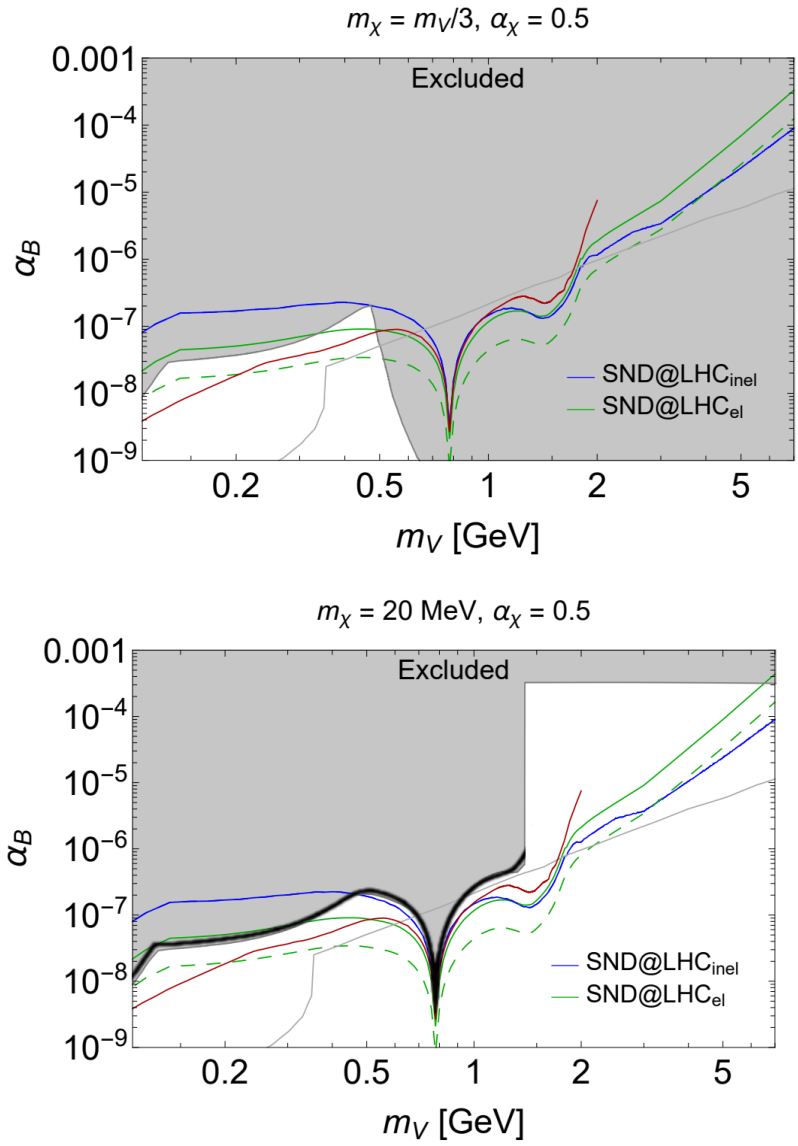

Figure 4.3: *Current constraints on DM particles and the sensitivity of several experiments plotted in two graphs with different m_χ. The upper graph has $m_\chi = m_V/3$. Therefore, from $m_V = 480\ MeV$ on, the constraints from CRESST-III are valid (see Appendix B). For $m_\chi = 20\ MeV < 160\ MeV$, which is shown in the lower graph, there is no constraint from CREST-III. Instead, for $m_V \gtrsim 1.5\ GeV$, the only constraint comes from CDF. The constraints seen in the lower (and partially the upper) graph for m_V up to 1.5 GeV come from MiniBooNE, indicated by the black line. The blue and light green lines show the sensitivity of SND@LHC for the inelastic (requiring $\gtrsim 100$ events) and elastic signature (plotted for 10 events) respectively. Plots taken from [3], with the addition of the black line from [13].*

Chapter 5

Advanced Configurations of SND

5.1 Events

In some more detail, the expected number of events during a run of the SND is given by

$$N_{events} = N^{LHC}_{produced,\chi\overline{\chi}} \cdot \epsilon^{SND}_{geom} \cdot n \cdot l \cdot \int \sigma(E_\chi) f^{\epsilon}_{\chi}(E_\chi) dE_\chi \tag{5.1}$$

where

- $N^{LHC}_{produced,\chi\overline{\chi}}$ is the total number of produced $\chi, \overline{\chi}$ particles at LHC in any direction during the whole run,
- ϵ^{SND}_{geom} is the geometric acceptance of the detector (i.e. the percentage of $\chi, \overline{\chi}$ particles that reach the detector),
- n is the number density of the target,
- l is the length of the detector and
- $\int \sigma(E_\chi) f^{\epsilon}_{\chi}(E_\chi) dE_\chi$ is the average cross section.

Regarding the average cross section, one could approximate $\int \sigma(E_\chi) f^{\epsilon}_{\chi}(E_\chi) dE_\chi = < \sigma > \approx \sigma(< E_\chi >)$. Of course the most accurate is to obtain an average cross section by weighing the cross section for a certain DM energy with the relative amount of particles with such an energy arriving at the detector ($\int \sigma(E_\chi) f^{\epsilon}_{\chi}(E_\chi) dE_\chi$). However, the approximation may be used if the cross section does not differ too much for the relevant energy range, such that the average cross section will simply be the cross section associated with the average energy of DM particles arriving at the detector.

Version of July 13, 2022– Created July 13, 2022 - 16:12

5.2 Advanced configurations

As has been stated in the introduction, two advanced set ups for the SND detector have been suggested. To examine how many events are to be expected for these configurations, the ratios of the components of eq. 5.1 with respect to the current (baseline, bl, SND@LHC) configuration is examined. The target remains composed of the same material, such that the number density and the mass density do not change. The advanced configurations are proposed for Run 4 of the LHC (which will then be the High Luminosity LHC) and will have instant luminosity 20 times as high as the current SND@LHC experiment. Other properties that influence the expected number of events are listed in Table 5.1.* One of the configurations, called $AdvSND_{far}$ is in (roughly) the same pseudorapidity range as the baseline configuration $SND@LHC$, which makes it very easy to obtain a good estimate for the amount of events. The other configuration, $AdvSND_{near}$, has a different pseudorapidity range, such that more elaborate calculations have to be performed.†

Table 5.1: *Properties of SND configurations*

Configuration	target cross section	distance l_{min}	η	target mass
SND@LHC	39 x 39 cm^2	480 m	[7.2, 8.6]	800 kg
$AdvSND_{far}$	100 x 55 cm^2	630 m	$\approx$ [7.2, 8.4]	5000 kg
$AdvSND_{near}$	120 x 120 cm^2	55 m	$\approx$ [4, 5]	5000 kg

5.2.1 $AdvSND_{far}$

Because $AdvSND_{far}$ is proposed to be in (roughly) the same pseudorapidity range as SND@LHC, the ratio between their geometric acceptances can be accurately approximated by the ratio between their solid angles. Because both configurations are in the far-forward regime, this ratio is (using the values from Table 5.1):

$$\frac{\epsilon^{far}_{geom}}{\epsilon^{bl}_{geom}} = \frac{\Omega^{far}}{\Omega^{bl}} = \frac{S^{far}}{S^{bl}}\left(\frac{d^{bl}}{d^{far}}\right)^2 = \frac{5500\ cm^2}{1521\ cm^2}\left(\frac{480\ m}{630\ m}\right)^2 \approx 2.1 \tag{5.2}$$

*Values from [15].

†I remind the reader that Appendix A contains a discussion of the pseudorapidity.

Because the mass density of the target does not change, the lengths ratio may be obtained from equating the mass density of the baseline and Adv_{far} configurations:

$$\frac{l^{far}}{l^{bl}} = \frac{m^{far}}{m^{bl}} \frac{A^{bl}}{A^{far}} = \frac{5000\ kg}{800\ kg} \frac{1521\ cm^2}{5500\ cm^2} \approx 1.7 \tag{5.3}$$

As $\text{AdvSND}_{\text{far}}$ has 20 times higher luminosity then SND@LHC,

$$N^{AdvSND_{far}}_{produced,\chi\overline{\chi}} = 20 \cdot N^{SND@LHC}_{produced,\chi\overline{\chi}} \tag{5.4}$$

Because both $\text{AdvSND}_{\text{far}}$ and SND@LHC are in the same pseudorapidity range, a justifiable assumption is that the average cross section is equal. Putting this all together, one obtains:

$$\begin{aligned} N^{AdvSND_{far}}_{events} &= 20 \cdot \frac{S^{far}}{S^{bl}} (\frac{d^{bl}}{d^{far}})^2 \frac{m^{far}}{m^{bl}} \frac{A^{bl}}{A^{far}} N^{SND@LHC}_{events} \\ &= 20 \cdot \frac{m^{far}}{m^{bl}} (\frac{d^{bl}}{d^{far}})^2 N^{SND@LHC}_{events} \\ &= 20 \cdot \frac{5000\ kg}{800\ kg} (\frac{480\ m}{630\ m})^2 N^{SND@LHC}_{events} \\ N^{AdvSND_{far}}_{events} &\approx 73 \cdot N^{SND@LHC}_{events} \end{aligned} \tag{5.5}$$

So, 73 times as many events are expected at $AdvSND_{far}$ compared to SND@LHC, regardless of the mediator mass.

5.2.2 Cross section

For the $\text{AdvSND}_{\text{near}}$ configuration, because the pseudorapidity range deviates significantly from the baseline configuration, the cross section has to be considered as well. To do so, a data set containing cross sections for dark matter particles with energy between 0 and 8 TeV has been analysed.‡ The cross section depends not only on the DM energy, but also the mediator mass. For the purpose of this research, the data for 2 GeV and 7 GeV has been used. Given the data, a fit of type $\sigma = a + b \cdot (E_{DM})^c$ has been made with scipy.optimize.curve_fit(). Figures 5.1 and 5.2 show the data and the fit for mediator masses m_V of 2 and 7 GeV respectively.

‡Data comes from [3].

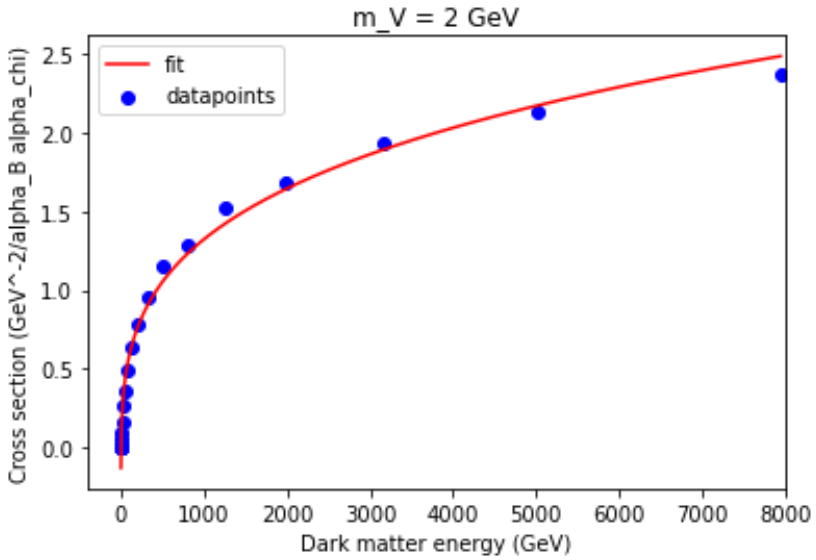

Figure 5.1: *Cross section as a function of the energy of a dark matter particle arriving at the detector, for a mediator mass of 2 GeV. Curve_fit gives (rounded off)* $a = -0.34 \pm 0.07$, $b = 0.28 \pm 0.05$, $c = 0.26 \pm 0.02$ *as best fit for* $\sigma = a + b \cdot (E_{DM})^c$.

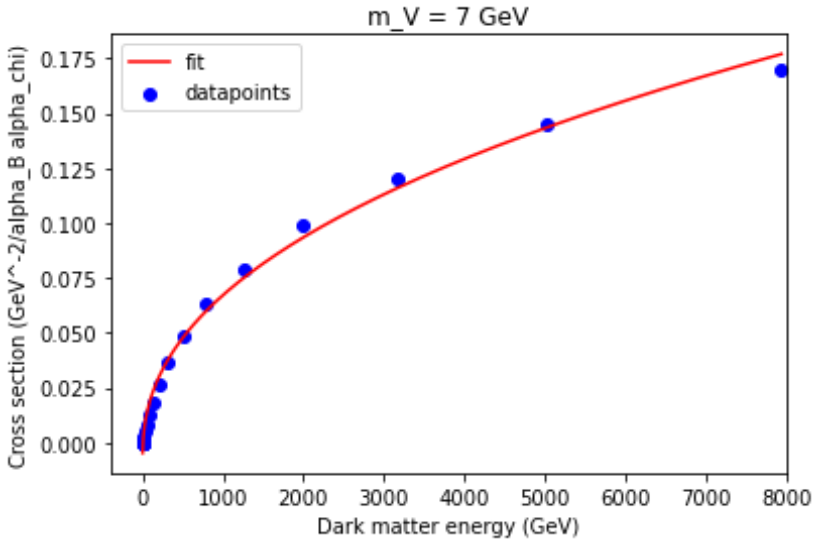

Figure 5.2: *Cross section as a function of the energy of a dark matter particle arriving at the detector, for a mediator mass of 7 GeV. Curve_fit gives (rounded off)* $a = -0.007 \pm 0.002$, $b = 0.0036 \pm 0.0006$, $c = 0.44 \pm 0.02$ *as best fit for* $\sigma = a + b \cdot (E_{DM})^c$.

5.2.3 Geometric Acceptance

Let us now turn to the geometric acceptances of the three configurations. Based on computations considered in [3], the percentage of particles arriving at the detector has been modelled. For completeness, the $AdvSND_{far}$ detector has also been included in the following considerations.

The data sets include 300,000 'particles' with their x,y and z momenta. The mass of the DM particles is assumed to be $m_\chi = 20\ MeV$ for both data sets, such that the energy of each particle can also be computed (and is included in the data set). The pseudorapidity of the particles (see eq. A.1) is determined. Those particles with pseudorapidity within the range of the detector (and positive p_z) are selected. Additionally, the total area corresponding to the pseudorapidity range of the relevant detector is calculated. The ratio between the area of the detector and the total area of the pseudorapidity range is calculated, using the values from Table 5.1. The percentage of particles arriving at the detector is now computed by multiplying the amount of particles in the pseudorapidity range with the area ratio and dividing by the total of 300,000 particles. In formula form, this looks like:

$$r_{detector} = \frac{N_{in\ \eta\ range}}{300,000} \frac{A_{detector}}{A_{\eta\ range}} \cdot 100\% \tag{5.6}$$

The geometric acceptances for the three SND configurations are given in Table 5.2 for mediator masses m_V of 2 and 7 GeV. It is interesting to note that for the AdvSND$_{near}$ configuration, the geometric acceptance is higher for a higher mediator mass, while for the SND@LHC and AdvSND$_{far}$ configurations, it is (way) lower. The reason is that we consider DM production by $V \rightarrow \chi\overline{\chi}$. During the pair production, the mass of the mediator is converted to transverse momentum of the DM particles. Therefore, a higher m_V means a higher p_T. As a result, there will be relatively more particles arriving at a lower pseudorapidity. As the total energy of the mediator must be very high in order to reach high pseudorapidity values, the geometric acceptance in the far forward regime decreases drastically.

Version of July 13, 2022– Created July 13, 2022 - 16:12

Table 5.2: *Geometric acceptance (percentage of produced DM particles arriving at the detector) and average energy of the arriving particles at the detector for the current configuration SND@LHC and the proposed configurations AdvSND$_{far}$ and AdvSND$_{near}$. The values are shown for mediator masses m_V = 2 & 7 GeV.*

Configuration ↓	Geometric acceptance		Average energy	
$m_V \rightarrow$	2 GeV	7 GeV	2 GeV	7 GeV
SND@LHC	1.72 %	0.08 %	1195.8 GeV	2319.9 GeV
AdvSND$_{far}$	3.44 %	0.16 %	1119.7 GeV	2313.9 GeV
AdvSND$_{near}$	0.41 %	0.95 %	43.9 GeV	146.5 GeV

5.2.4 Average cross section

For the selected particles (arriving in the pseudorapidity range of the detector), the average energy is calculated and reported in Table 5.2. With the average energy of the particles arriving at the detector, a rough estimate of the cross section can be made by stating:

$$\int \sigma(E_\chi) f_\chi^\epsilon(E_\chi) dE_\chi = <\sigma> \approx \sigma(<E_\chi>) \tag{5.7}$$

as discussed earlier. By using the average energies from Table 5.3 and the fit parameters from Figures 5.1 & 5.2, $\sigma(<E_\chi>)$ can be computed. The results are shown in Tab. 5.3.

Table 5.3: *Average energy of the arriving particles at the detector as well as the average cross section for the current configuration SND@LHC and the proposed configurations AdvSND$_{far}$ and AdvSND$_{near}$. The values are shown for mediator masses m_V = 2 & 7 GeV.*

Configuration ↓	Average energy (GeV)		Average σ $(GeV^{-2}/\alpha_B\alpha_\chi)$	
$m_V \rightarrow$	2 GeV	7 GeV	2 GeV	7 GeV
SND@LHC	1195.8	2319.9	1.40	0.10
AdvSND$_{far}$	1119.7	2313.9	1.37	0.10
AdvSND$_{near}$	43.9	146.5	0.41	0.03

5.2.5 AdvSND$_{\text{near}}$

Now that all components of eq. 5.1 have been considered, the following conclusion can be drawn:

$$
\begin{aligned}
N_{events}^{AdvSND_{near}} &= \frac{N^{AdvSND_{near}\,produced,\chi\bar{\chi}}}{N^{SND@LHC_{produced,\chi\bar{\chi}}}} \frac{\epsilon_{geom}^{AdvSND_{near}}}{\epsilon_{geom}^{SND@LHC}} \frac{l^{AdvSND_{near}}}{l^{SND@LHC}} \frac{<\sigma>^{AdvSND_{near}}}{<\sigma>^{SND@LHC}} N_{events}^{SND@LHC} \\
&= 20 \cdot \frac{\epsilon_{geom}^{AdvSND_{near}}}{\epsilon_{geom}^{SND@LHC}} \frac{m^{AdvSND_{near}}}{m^{SND@LHC}} \frac{A^{SND@LHC}}{A^{AdvSND_{near}}} \frac{<\sigma>^{AdvSND_{near}}}{<\sigma>^{SND@LHC}} N_{events}^{SND@LHC} \\
&\overset{2\ GeV}{=} 20 \cdot \frac{0.41}{1.72} \frac{5000\ kg}{800\ kg} \frac{1521\ cm^2}{14400\ cm^2} \frac{0.41}{1.40} N_{events}^{SND@LHC} \\
&\overset{7\ GeV}{=} 20 \cdot \frac{0.95}{0.08} \frac{5000\ kg}{800\ kg} \frac{1521\ cm^2}{14400\ cm^2} \frac{0.03}{0.10} N_{events}^{SND@LHC}
\end{aligned}
\tag{5.8}
$$

So, for a mediator mass $m_V = 2\ GeV$, $N_{events}^{AdvSND_{near}} \approx 0.9 \cdot N_{events}^{SND@LHC}$, while for a mediator mass $m_V = 7\ GeV$, $N_{events}^{AdvSND_{near}} \approx 47 \cdot N_{events}^{SND@LHC}$.

5.2.6 Sensitivity

If we recall

$$
\sigma_{total} = \sqrt{\sigma_{Poisson}^2 + \sigma_{experimental}^2} = \sqrt{N_{NC} + (\epsilon \cdot N_{NC})^2} \tag{5.9}
$$

we can estimate the sensitivity of the advanced configurations to probe the NC/CC signature. Because the error σ scales with N_{NC}, the sensitivity remains unchanged if ϵ remains unchanged. However, the components of the advanced configurations will have improved, such that the sensitivity is actually higher for the advanced configurations. Assuming $\epsilon = 1$ % instead of 10 % and using the value from eq. 5.5 and $N_{NC}^{bl} = 450$, we obtain:

$$
\sigma_{total}^{advSND_{far}} = \sqrt{73 \cdot N_{NC}^{bl} + (0.01 \cdot 73 \cdot N_{NC}^{bl})^2} \approx 375
$$

so $2\sigma^{AdvSND_{far}} = 750 = 7.5 \cdot 2\sigma^{SND@LHC}$ while there are about 73 times as many events. Therefore, the sensitivity of AdvSND$_{far}$ is better.

At AdvSND$_{near}$, 1685 neutrino DIS events are expected. Because we know the NC/CC ratio to be 0.33 (see 3.2.2), we know that 25 % of the neutrino events will be NC events. Therefore, a 2σ confidence level would require:

$$
2\sigma^{AdvSND_{near}} = 2\sqrt{1685 \cdot 0.25 + (0.01 \cdot 1685 \cdot 0.25)^2} \approx 42 \tag{5.10}
$$

This is less than the 100 events required for SND@LHC and way less than the 750 events required for AdvSND$_{far}$. For a mediator mass of 7 GeV, 47 times as many DM DIS events are expected at AdvSND$_{far}$ as compared to SND@LHC, so for such a mediator mass, AdvSND$_{near}$ would be the most efficient.

5.3 Discussion

Firstly, the results for the average cross section in Table 5.3 show that the assumptions made in 5.2.1 were indeed justified.

With regards to the calculated values for the $AdvSND_{near}$ configuration, it must be noted that those are the most uncertain, because its pseudorapidity range is the least accurate ($\approx [4, 5]$). To illustrate this, the calculations have also been performed for pseudorapidity ranges [3.6, 4.6] and [4.4, 5.4]. The results are given in Table 5.4.

Table 5.4: *Geometric acceptance (percentage of produced DM particles arriving at the detector) and average energy of the arriving particles at the detector for three eta ranges of AdvSND$_{near}$. The values are shown for mediator masses m_V = 2 & 7 GeV.*

η range $\downarrow$	Geometric acceptance		Average energy	
$m_V \rightarrow$	2 GeV	7 GeV	2 GeV	7 GeV
(4,5)	0.41 %	0.95 %	43.9 GeV	146.5 GeV
(3.6,4.6)	0.15 %	0.42 %	29.5 GeV	98.1 GeV
(4.4,5.4)	1.14 %	2.14 %	64.9 GeV	218.6 GeV

Although the cross section does not change that much for these alternative average energies, Table 5.4 shows that the geometric acceptances are influenced quite strongly by differing the pseudorapidity range. Therefore, the calculated values for AdvSND$_{near}$ must be treated with caution.

Both the method for obtaining the geometric acceptance and the method for obtaining the cross section can be improved. Currently, the geometric acceptance is determined by considering the whole pseudorapidity range as 1 bin and multiplying the amount of particles that end up in this bin by the ratio between the area of the detector and the area covered by the pseudorapidity range. However, it would be more accurate to divide the pseudorapidity range into more bins (or even obtain a probability density

function with respect to η) and consider what portion of the detector's area lies in this pseudorapidity range. This would matter because the amount of particles depends on η, as is illustrated for the 2 GeV case in Fig. 5.3.

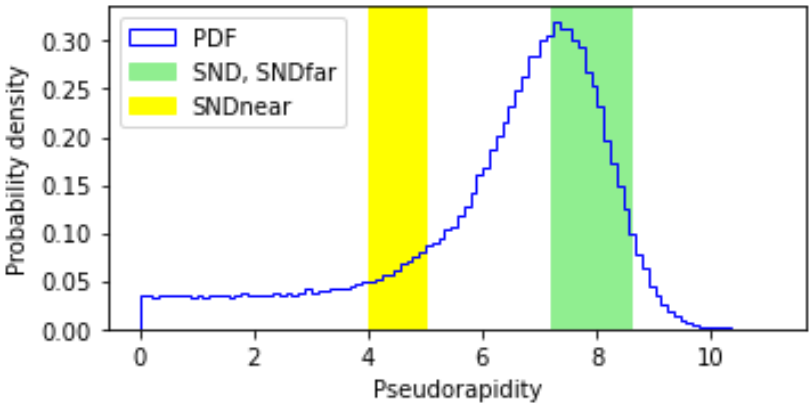

Figure 5.3: *Probability density function (histogram) for particles to have a certain pseudorapidity. This plot is based on the 2 GeV data set. One can see that for the pseudorapidity ranges of interest for the three considered configurations, the probability to find a particles depends on η. (Please note that the shape is quite different for a mediator mass of 7 GeV.)*

The same reasoning applies to the cross section being based on the average energy. It would be more accurate to obtain a probability density function for a particle within the pseudorapidity range of the detector to have a certain energy, and integrate the function with the cross section function (based on the fitting procedure above). Especially for the AdvSND$_{near}$ configuration, this could make a difference, as it can be seen in Fig. 5.1 that the cross section changes rapidly with the DM energy for low DM energies (as is the case for the AdvSND$_{near}$ configuration).

Nevertheless, it can be concluded that AdvSND$_{far}$ will have a higher sensitivity than SND@LHC in any case and AdvSND$_{near}$ may have even higher sensitivity, depending on the mediator mass.

Chapter 6

Conclusion

SND@LHC is a neutrino detector at the Large Hadron Collider that may also probe dark matter candidates. A leptophobic portal has been considered. The SND experiment covers parts of the parameter space that have not yet been excluded by previous experiments. For the two advanced configurations considered in this research, AdvSND$_{far}$ will have a better sensitivity to probe DM in the NC/CC signature than SND@LHC for any mediator mass, as the amount of DM DIS events increases more than the required amount of events to reach the 2σ confidence level. For AdvSND$_{near}$, this depends on the mediator mass. For the mediator masses considered in this research, AdvSND$_{near}$ has a better sensitivity than SND@LHC for both $m_V = 2$ and 7 GeV. However, for 2 GeV the sensitivity of AdvSND$_{far}$ is better, while for 7 GeV, the sensitivity of AdvSND$_{near}$ is better. This being said, the absolute sensitivity remains uncertain, because the amount of neutrino events is uncertain.

Acknowledgements

I would like to thank my supervisor Maksym Ovchynnikov for introducing me to the wondrous world of particle physics. Most of the literature was incomprehensible to me at the beginning of this research project, but after all his explanations, I am now able to understand the basics. Also, I would like to thank Florian Reindl from the CRESST collaboration for providing crucial details to understand the CRESST-III 160 MeV bound.

Bibliography

[1] A. Boyarsky, O. Ruchayskiy, D. Iakubovskyi, and J. Franse, *Unidentified Line in X-Ray Spectra of the Andromeda Galaxy and Perseus Galaxy Cluster*, Physical Review Letters **113**, 251301 (2014).

[2] K. Bondarenko, A. Boyarsky, M. Ovchynnikov, and O. Ruchayskiy, *Sensitivity of the intensity frontier experiments for neutrino and scalar portals: analytic estimates*, Journal of High Energy Physics **2019** (2019).

[3] A. Boyarsky, O. Mikulenko, M. Ovchynnikov, and L. Shchutska, *Searches for new physics at SND@LHC*, Journal of High Energy Physics **2022** (2022).

[4] K. Bondarenko, *Plan B for particle physics : finding long lived particles at CERN*, PhD thesis, Leiden University, 2018.

[5] B. W. Lee and S. Weinberg, *Cosmological Lower Bound on Heavy-Neutrino Masses*, Physical Review Letters **39**, 165 (1977).

[6] C. Ahdida et al., *Scattering and Neutrino Detector at the LHC*, Technical report, CERN, Geneva, 2020.

[7] C. Ahdida et al., *SND@LHC - Scattering and Neutrino Detector at the LHC*, Technical report, CERN, Geneva, 2021.

[8] E. A. Paschos, *Precise Ratios for Neutrino-Nucleon and Neutrino-Nucleus Interactions*, 2002.

[9] S. Alekhin et al., *A facility to search for hidden particles at the CERN SPS: the SHiP physics case*, Reports on Progress in Physics **79**, 124201 (2016).

[10] F. Hamlin, *Implications of the neutrino NC/CC ratio measured by SND@LHC*, Bachelor's thesis, Leiden University, 2021.

[11] S. Naaz, J. Singh, and R. B. Singh, *DUNE Prospect for Leptophobic Dark Matter*, Advances in High Energy Physics **2020**, 1 (2020).

[12] A. Abdelhameed et al., *First results from the CRESST-III low-mass dark matter program*, Physical Review D **100** (2019).

[13] A. A. Aguilar-Arevalo et al., *Dark matter search in nucleon, pion, and electron channels from a proton beam dump with MiniBooNE*, Phys. Rev. D **98**, 112004 (2018).

[14] T. Aaltonen et al., *Search for dark matter in events with one jet and missing transverse energy in $p\overline{p}$ collisions at $\sqrt{s} = 1.96$ TeV*, Physical review letters **108** (2012).

[15] J. L. Feng et al., *The Forward Physics Facility at the High-Luminosity LHC*, 2022.

[16] P. M. M. Bauer, *Data analysis for the CRESST experiment: New methods, improved alpha analysis, and results on light dark matter and backgrounds*, PhD thesis, Munich University of Technology, 2020.

[17] A. H. Abdelhameed et al., *Description of CRESST-III Data*, 2019.

Appendix A

Pseudorapidity

Pseudorapidity, η, is used in particle physics to describe the angle of a particle trajectory with respect to some axis (the pre-collision beam). It is defined as

$$\begin{aligned} \eta &= -ln(tan(\frac{\theta}{2})) \\ &= arctanh(\frac{p_L}{|\vec{p}|}) \end{aligned} \tag{A.1}$$

where p_L is the momentum component along the beam axis. As can be seen from these formulae and in Fig. A.1, an angle of 0 degrees corresponds to infinite pseudorapidity, an angle of 90 degrees corresponds to zero pseudorapidity. High pseudorapidity range corresponds to the far-forward regime, particles with most of their momentum in the forward direction (along the beam axis).

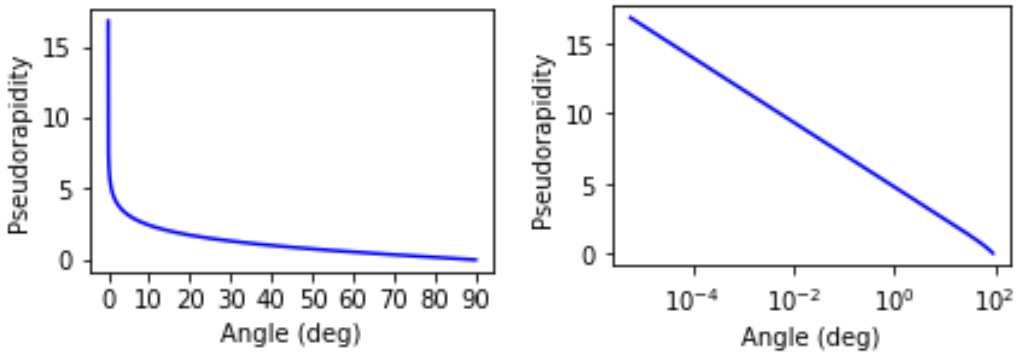

Figure A.1: *Pseudorapidity as a function of the angle of a particle trajectory with respect to the beam axis. On the left, the x-scale is plotted linearly, showing that the pseudorapidity drastically increases for angles smaller than about 1°. On the right, the x-axis is plotted logarithmically.*

Appendix B

m_χ limit CRESST-III

Besides a plot indicatingThis appendix provides a complete derivation for a DM particle χ scattering elastically with a particle β. β will be the nucleus of an atom in the target material used at the CRESST-III experiment.

$$\chi + \beta \rightarrow \chi^{'} + \beta^{'}$$

I assume all speeds are non-relativistic and the β particle is at rest before the interaction. As will be seen in eq. B.13 the speed of the DM particles is less then 1000 km/s, so this assumption can indeed be made.

Let us introduce (in the lab frame, where $E_\beta = m_\beta$ since I assume it stationary):

$$E_{transfer} = E_{\beta'} - E_\beta = E_{\beta'} - m_\beta$$

Momentum conservation dictates:

$$(p_\chi - p_{\chi'})^2 = (p_{\beta'} - p_\beta)^2 \tag{B.1}$$

Since quantities $p_\mu p^\mu$ are Lorentz invariant, we can choose to evaluate one side of the equation in the center-of-momentum frame, while evaluating the other side in the laboratory frame, where β is at rest, using $p_\beta^{lab} = (m_\beta, 0, 0, 0)$

$$\begin{aligned}(p_{\beta'} - p_\beta)^2 &= p_{\beta'}^2 + p_\beta^2 - 2p_{\beta'}p_\beta = m_{\beta'}^2 + m_\beta^2 - 2p_{\beta'}p_\beta \\ &\overset{lab}{=} 2m_\beta^2 - 2E_{\beta'}^{lab} m_\beta = 2m_\beta(m_\beta - E_{\beta'}^{lab}) = -2m_\beta E_{transfer}\end{aligned} \tag{B.2}$$

Let us now turn to the COM(cm) frame, where we know that $|\vec{p_\chi}| = |\vec{p_\beta}|$ and $|\vec{p_{\chi'}}| = |\vec{p_{\beta'}}|$ such that the total momentum before and after the collision is zero. As a result, $|\vec{p_{\chi'}}| = |\vec{p_\chi}|$ and $E^{cm}_{\chi'} = E^{cm}_\chi = \sqrt{|\vec{p_\chi}^{\,cm}|^2 + m^2_\chi}$.

$$\begin{aligned}
(p_\chi - p_{\chi'})^2 &= m^2_\chi + m^2_{\chi'} - 2p_\chi p_{\chi'} \\
&= 2m^2_\chi - 2E_\chi E_{\chi'} + 2\vec{p_\chi}\cdot\vec{p_{\chi'}} \\
&= 2m^2_\chi - 2E_\chi E_{\chi'} + 2|\vec{p_\chi}||\vec{p_{\chi'}}|cos(\theta) \\
&\overset{cm}{=} 2m^2_\chi - 2E^{cm}_\chi E^{cm}_{\chi'} + 2|\vec{p_\chi}^{\,cm}||\vec{p_{\chi'}}^{\,cm}|cos(\theta) \\
&= 2m^2_\chi - 2E^{cm}_\chi E^{cm}_\chi + 2|\vec{p_\chi}^{\,cm}|^2 cos(\theta) \\
&= 2m^2_\chi - 2(|\vec{p_\chi}^{\,cm}|^2 + m^2_\chi) + 2|\vec{p_\chi}^{\,cm}|^2 cos(\theta) \\
&= -2|\vec{p_\chi}^{\,cm}|^2(1 - cos(\theta)) \\
&= -4|\vec{p_\chi}^{\,cm}|^2 sin(\frac{\theta}{2})^2
\end{aligned} \tag{B.3}$$

Equating B.3 and B.2 yields

$$\begin{aligned}
-2m_\beta E_{transfer} &= -4|\vec{p_\chi}^{\,cm}|^2 sin(\frac{\theta}{2})^2 \\
E_{transfer} &= 2\frac{|\vec{p_\chi}^{\,cm}|^2}{m_\beta} sin(\frac{\theta}{2})^2
\end{aligned} \tag{B.4}$$

What is left, is to figure out $|\vec{p_\chi}^{\,cm}|$

$$m_\chi v^{cm}_\chi = m_\beta v^{cm}_\beta \rightarrow v^{cm}_\beta = \frac{m_\chi}{m_\beta} v^{cm}_\chi \tag{B.5}$$

We make a transformation between the lab frame, where $v^{lab}_\beta = 0$ and the COM frame, where $v^{cm}_\beta = \frac{m_\chi}{m_\beta} v^{cm}_\chi$. As this velocity is non-relativistic, we can say $v_{trans} = \frac{m_\chi}{m_\beta} v^{cm}_\chi$ such that

$$v^{cm}_\chi = v^{lab}_\chi - v_{trans} = v^{lab}_\chi - \frac{m_\chi}{m_\beta} v^{cm}_\chi \tag{B.6}$$

so

$$v^{cm}_\chi = \frac{v^{lab}_\chi}{1 + \frac{m_\chi}{m_\beta}} \tag{B.7}$$

Version of July 13, 2022– Created July 13, 2022 - 16:12

so

$$|\vec{p_\chi}^{cm}| = m_\chi v_\chi^{cm} = \frac{m_\chi v_\chi^{lab}}{1+\frac{m_\chi}{m_\beta}} \tag{B.8}$$

Therefore,

$$\frac{E_{transfer}}{sin(\frac{\theta}{2})^2} = 2\frac{|\vec{p_\chi}^{cm}|^2}{m_\beta} = 2\frac{m_\chi^2 (v_\chi^{lab})^2}{m_\beta (1+\frac{m_\chi}{m_\beta})^2} = 2\frac{m_\beta m_\chi^2 (v_\chi^{lab})^2}{(m_\beta+m_\chi)^2} \tag{B.9}$$

We see that the energy transfer's maximum is at $sin(\frac{\theta}{2}) = 1$ so we may say:

$$E_t = E_{transfer,max} = 2\frac{m_\beta m_\chi^2 (v_\chi^{lab})^2}{(m_\beta+m_\chi)^2} \tag{B.10}$$

Let us now rewrite this to obtain an equation for m_χ in terms of E_t:

$$m_\chi^2 E_t + 2m_\chi m_\beta E_t + m_\beta^2 E_t - 2m_\chi^2 m_\beta (v_\chi^{lab})^2 = 0 \tag{B.11}$$

So, using the abc-formula:

$$\begin{aligned} m_\chi &= \frac{-2m_\beta E_t \pm \sqrt{4m_\beta^2 E_t^2 - 4(E_t - 2m_\beta (v_\chi^{lab})^2) m_\beta^2 E_t}}{2(E_t - 2m_\beta (v_\chi^{lab})^2)} \\ &= \frac{m_\beta E_t + \sqrt{2m_\beta^3 E_t (v_\chi^{lab})^2}}{2m_\beta (v_\chi^{lab})^2 - E_t} \\ &= \frac{m_\beta E_t + \sqrt{2E_t} m_\beta^{3/2} v_\chi^{lab}}{2m_\beta (v_\chi^{lab})^2 - E_t} \end{aligned} \tag{B.12}$$

The target at CRESST-III is $CaWO_4$ [12](Oxygen has the lightest mass, Tungsten the heaviest), so to obtain the maximum momentum transfer, take the Oxygen nucleus. v_χ^{lab} is given by the escape velocity of the dark matter particles, the velocity of the Sun around the Milkyway and the velocity of the Earth around the Sun. The nuclear recoil threshold in CRESST-III is 30.1 eV. Therefore, let us now plug in the following values (also used by the CRESTT colaboration [16]):

$$v_\chi^{lab} = v_{esc}^{Milkyway} + v_{Sun-MW} + v_{Earth-Sun} = 544 + 231 + 30\,km/s = 0.002685c \tag{B.13}$$

$$m_\beta = m_{Oxygen} = 1.4903 \cdot 10^{10}\ eV/c^2 \tag{B.14}$$

However, plugging in these values yields (for $E_{transfer} \approx 30\ eV$): $m_\chi \approx 180\ MeV/c^2$, which is quite different from the 160 MeV presented in [12].

The explanation for this discrepancy is the $E_{transfer}$ that is used. In reality, the detector is not ideal and does not have perfect energy resolution. 30.1 eV is only the mean value of the Gaussian distribution describing the energy threshold. It has $\sigma = 4.6\ eV$ [17]. Therefore, the 30.1 eV is not necessarily the lowest recoil energy that can be detected. In the thesis of P. Bauer [16], it is stated that the energy threshold (30.0 eV) has a systematic error of -6.5. Using 23.5 eV yields $m_\chi \approx 160\ MeV$.

Constraints posed by CRESST-III

Figure B.1 shows the results of the CRESST-III experiment from [12]. The plot clearly shows that the experiment has probed DM particles down to $m_\chi \approx 160\ MeV$. For the $m_\chi = m_V/3$ choice considered in Fig. 4.3, this corresponds to $m_V \approx 480\ MeV$.

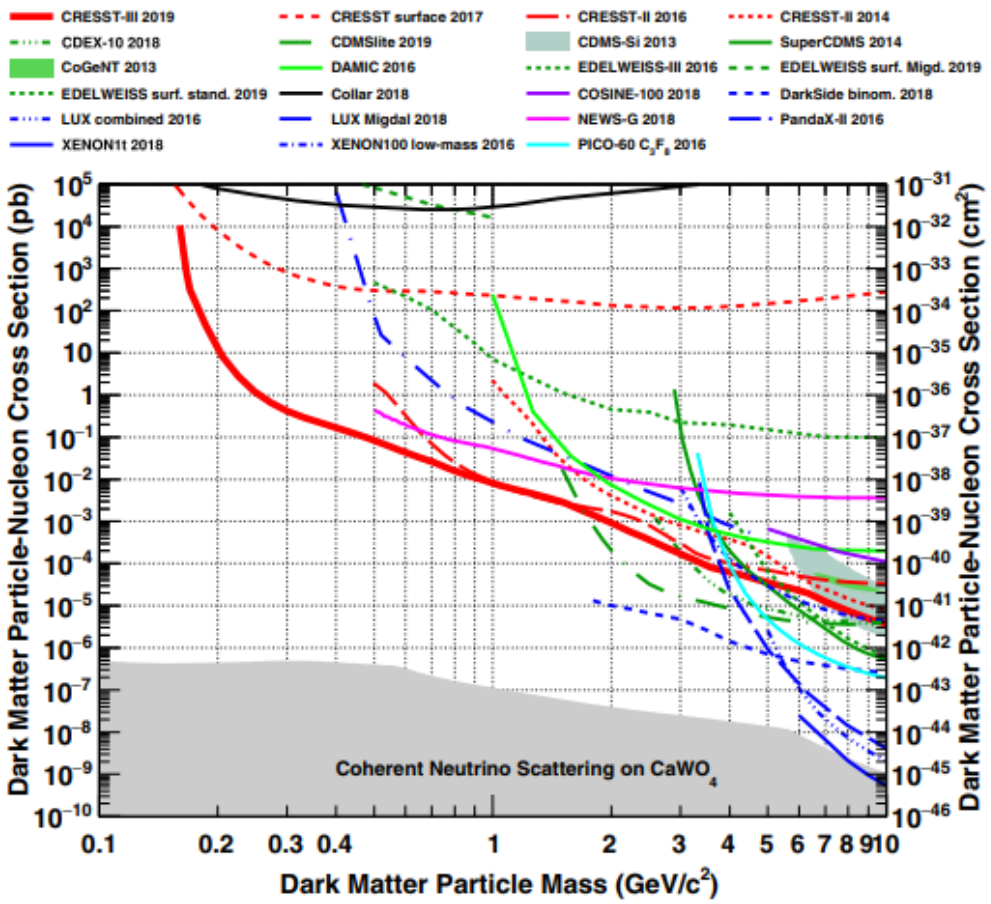

Figure B.1: *Plot from [12] indicating the DM-nucleon cross section vs the DM particle mass. The red line shows that for DM particle mass below 1 GeV CRESST-III has increased the constraints on DM models.*